Catalysis Science & Technology

Accepted Manuscript

ROYAL SOCIETY OF CHEMISTRY

www.rsc.org/catalysis

Identifying active sites of CoNC/CNT from pyrolysis of molecularly defined complexes for oxidative esterification and hydrogenation reactions

Tianyuan Cheng[a], Hao Yu[*a], Feng Peng[a], Hongjuan Wang[a], Bingsen Zhang[*b], Dangsheng Su[b]

[a] *School of Chemistry and Chemical Engineering, South China University of Technology, Guangzhou 510640, P.R. China*

[b] *Catalysis and Materials Division, Shenyang National Laboratory for Materials Science, Institute of Metal Research, Chinese Academy of Sciences, Shenyang 110016, P.R. China*

[*] To whom correspondence should be addressed.
yuhao@scut.edu.cn (H Yu), Tel.: +86 20 87114916, Fax.: + 86 20 87114916;
bszhang@imr.ac.cn (BS Zhang), Tel.: +86 24 83970027

Abstract

As an emerging catalyst based on earth-abundant metals, Co_3O_4 supported on carbon materials, derived from the pyrolysis of metal salts and nitrogen-containing ligands, shows excellent performances in hydrogenation, hydrogenated coupling, oxidative esterification and oxidation of amines. Herein, we unravel the real active sites of this catalyst through a combination of XRD, XPS, HRTEM, EELS and poisoning experiments with sulfur-containing compounds. The oxidative esterification of benzyl alcohol, nitrobenzene hydrogenation and hydrogenated coupling of nitrobenzene with benzaldehyde were used as probe reactions. By comparing the catalytic performance before and after HCl washing, it was demonstrated that particulate Co_3O_4 has marginal effect on the catalysis, and the highly dispersed CoNx on carbon nanotubes created during the pyrolysis is responsible for the activity. It was proposed that cobalt chelate complexes bonded to 2 to 3 nitrogens in graphene lattice, probably like the pyridinic vacancy, might be responsible for the activity.

Keywords: CoNC; oxidative esterification; hydrogenation; hydrogenated coupling; energy-filtered transmission electron microscopy

1. Introduction

Catalysts are essential for chemical transformations in chemical and pharmaceutical industries. Numerous molecular catalysts with earth-abundant metals as core and proper ligands have been developed and applied in diverse chemical synthesis, such as oxidative esterification,[1, 2] hydrogenation reaction,[3, 4] epoxidation of olefins,[5-7] Diels-Alder reaction[8, 9] and so on. However, the homogeneous catalysts suffer from the difficulties in recycling and separation from products. To overcome the weakness, it is highly desirable to immobilize the molecular catalysts upon solid supports to form their heterogeneous versions without losing activity and specificity.

So far, various homogeneous catalysts have been immobilized on resins, zeolites, metal oxides, etc. by iron exchange,[10, 11] encapsulation,[12, 13] grafted[14, 15] and so on. Carbon materials are regarded as an excellent support, which can be chemically functionalized and/or decorated with metallic complexes and enzymes to improve catalytic activity or to act as biosensors.[16-18] Recently, a thermolysis approach has been proposed by Beller M. and co-workers for synthesizing iron / cobalt oxide catalysts on carbon blacks.[19-26] Through the pyrolysis of metal salts and nitrogen-containing ligands, represented by 1,10-phenanthroline, blended with carbon blacks, very active catalysts have been produced for the heterogeneous hydrogenation of nitroarenes,[20, 21] oxidation of amines for nitriles,[24] oxidative esterification of alcohols,[19] and hydrogenation coupling of carbonyl compounds.[23, 26] The heterogeneous catalysts are inexpensive, easily reusable and environmentally benign.

Despite these achievements, it currently remains unclear what exactly are the active sites of those emerging catalysts. In one of the early publications in this field, Westerhaus F.A. et al.[21] defined the structure of the hydrogenation catalyst, formed by pyrolysis of a cobalt-phenanthroline complex adsorbed on activated carbon, as Co_3O_4 particles with a very wide size distribution, on the surface of which three nitrogen atoms are statistically bound to one cobalt atom. A similar catalyst, Co_3O_4-N supported on Vulcan XC72R carbon black, was proved active in oxidative esterifications of alcohols.[19] In a recent work from Deng J et al., the formation of Co^0 during the pyrolysis was also emphasized.[27] In the case of iron oxide catalysts produced by the similar method, its excellent hydrogenation activity has been attributed to the formation of active Fe_2O_3 particles surrounded by 3-5 layers of nitrogen-doped graphene, on which FeNx structure can be detected.[20] Recently, Beller and co-workers defined these structures as a core-shell-structured metal oxide@N-doped graphene supported on carbon materials.[23, 26] Nevertheless, some fundamental issues on the nature of active sites are not be fully understood yet. It is still unclear what the role of metal oxide is. Whether and how the oxide core participates into the catalysis, as it is encapsulated in a carbon shell? Secondly, the previous works show that the active catalysts usually have a wide size distribution, from sub-nanometer structures to large particles over 100 nm. Are there any different catalytic behaviors on them? In addition, it deserves attentions to disclose the other possible types of active sites, because many compounds may be produced through the pyrolysis of a system containing transition metal, nitrogen and carbon, such as oxides,

nitrides, oxynitrides and carbonitrdes, analogized to the complicated cases of transition metal catalysts for the oxygen reduction reaction.[28]

In this work, an effort was made to identify the active sites responsible for the excellent activity of the CoNC/carbon. Carbon nanotubes (CNTs) were used as support to immobilize the Co complex by pyrolysis, because the well-defined structure and mesoporous feature of CNTs are beneficial for the unambiguous identification of cobalt species. The major concern was to evaluate the role of cobalt oxide, which can be selectively removed by acid, allowing for a comparative study on the catalysts with or without cobalt oxides. The catalysts were subjected to the oxidative esterification of benzyl alcohol by molecular oxygen, the selective reduction of nitrobenzene by hydrogen and the hydrogenated coupling of nitrobenzene and benzaldehyde as probe reactions. Across the spectrum of reactions, new insights into the active site of CoNC/CNT were revealed.

2. Experimental

2.1 Catalyst preparation

The CoNC/CNT catalyst was prepared as described in literature.[19] Typically, 125 mg of $Co(OAc)_2 \cdot 4H_2O$ and 198 mg of 1,10-phenanthroline (Co : phenanthroline = 1:2 (mol)) were dissolved in 30 mL ethanol and stirred for 30 min at room temperature. Then, 650mg CNTs (provided by Cnano Co. Ltd. as received, >99.9% purity, synthesized using a supported Fe catalyst) were added to form a suspension under agitation for 5 hours at 60 °C. After cooled to room temperature, the

suspension was dried at 70 °C for 12 h. The obtained solids were ground to fine powder, then were annealed at 800 °C for 2 h under flowing Ar at 100 $Ncm^3 \cdot min^{-1}$.

The CoNC/CNT catalyst was thoroughly washed with 2 M hydrochloric acid at room temperature for 5h. The resulting sample is denoted as CoNC/CNT-HCl. The CoNC/CNT catalyst was also washed with 9 M nitric acid at 120°C, and then annealed at 800 °C for 2 h. The resulting sample is denoted as CoNC/CNT-HNO_3.

For comparison, CNTs were replaced by carbon blacks (XC-72R) to synthesize the CoNC catalysts with same procedures. The resulting catalysts are denoted as CoNC/CB, CoNC/CB-HCl and CoNC/CB-HNO_3, respectively.

2.2 Catalyst Characterizations

Brunauer–Emmett–Teller (BET) specific surface areas (S_{BET}) were measured by N_2 adsorption at 77 K in an ASAP 2010 analyzer. X-ray diffraction (XRD) patterns were recorded on a Bruker D8 ADVANCE diffractometer equipped with a rotating anode using Cu Kα radiation (40 kV, 40 mA). X-ray photoelectron spectroscopy (XPS) was performed in a Kratos Axis ultra (DLD) spectrometer equipped with an AlKα X-ray source. The binding energies were referenced to the C1s peak at 284.8 eV. High-resolution transmission electron microscopy (HRTEM) images and electron energy loss spectroscopy (EELS) spectra were recorded by using a FEI Tecnai G2 F20 microscope. Raman spectra were recorded on a LabRAM Aramis micro Raman spectrometer with 633 nm wavelength laser and 2 μm spot size. Elemental analysis was taken using Vario EL III (Elementar, Germany). The contents of element Co were measured using atomic adsorption spectroscopy (Hitachi Z-5000). H_2S

temperature-programmed desorption (H_2S-TPD) was carried out in a TP5080 adsorption instrument equipped with a thermal conductivity detector (TCD) detector. Before H_2S-TPD experiments,~0.05 g samples were pretreated in N_2 (30 mL/min) at 300 °C for 1 h then were exposed to 1024 ppm H_2S/N_2 atmosphere at 200°C for 2 h. After purged with He at 50°C for additional 1 h, TPD profiles were recorded from room temperature to 600°C at a ramping rate of 10 °C min^{-1} under flowing He.

2.3 Catalytic test

The oxidative esterification of benzyl alcohol (BA) was carried out in a 60 ml stainless steel autoclave lined with Teflon to minimize the effect of metallic wall. 0.4 ml BA, 32 ml methanol, 1 ml anisole as internal standard, 0.1 g K_2CO_3 and 200 mg catalysts were added into the reactor and heated to 60 ^oC with stirring at 1000 rpm. Then O_2 (2 MPa) was fed into the reactor (defining t=0) to initiate the reaction. After a certain reaction duration, liquid products mixed with catalysts were transferred from the reactor to stop the reaction. The products were analyzed by gas chromatography (GC) with a HP-5 ms capillary column (30 m, DF = 0.25 mm, 0.25 mm i.d.).

For the hydrogenation of nitrobenzene (NB), 0.4 ml NB, 32 ml ethyl alcohol, 1 ml octane as internal standard and 200 mg catalysts were added into the reactor and heated to 110 ^oC with stirring at 1000 rpm. Then the hydrogenation reaction was carried out at 2 MPa H_2. For the hydrogenated coupling of NB and benzaldehyde (BDH), 0.4 ml NB, 1 ml BDH, 30 ml ethyl alcohol, 0.5 ml octane as internal standard and 400 mg catalysts were used. The reaction was carried out at 110 ^oC and 2 MPa H_2 with stirring at 1000 rpm.

The poisoning effects of KSCN and H_2S on the CoNC catalysts in the oxidative esterification of BA were investigated. In the case of KSCN as poisoner, 1 g KSCN was added into the reactants to conduct the reaction. In the case of H_2S, the catalyst was pretreated by flowing 1024 ppm H_2S/N_2 at 100 Ncm^3/min at 200 ^oC for 2 h in a horizontal tubular furnace.

3. Results and discussion

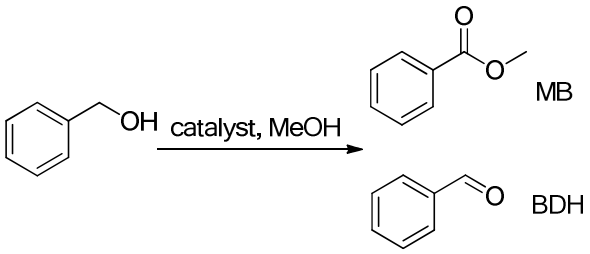

Scheme1.

Table 1. Catalytic performances of CoNC/CNT and CoNC/CB catalysts in the oxidative esterification of BA (Scheme 1) [a]

Entry	Catalysts	Composition Co/Fe/N (w%)	S_{BET} (m^2/g)	Conv. (%)	Selectivity (%) BDH	MB
1	Blank [b]	-	-	0	0	0
2	CoNC/CNT	1.81/-/1.42	155.9	88.1	8.4	91.6
3	CoNC/CNT-HCl	0.42/-/1.71	144.8	88.4	7.4	92.6
4	CoNC/CNT-HNO_3	0.14/-/0.31	210.0	42.1	14.5	85.5
5	CoNC/CB	3.01/-/n.d.	123.1	91.4	3.0	97.0
6	CoNC/CB-HCl	0.74/-/n.d.	109.8	81.8	5.7	94.3
7	CoNC/CB-HNO_3	0.05/-/n.d.	210.3	47.4	24.2	75.8
8	CNTs	-	204.1	0	0	0
9	NCNTs [c]	3.44 [d]	60.4	0	0	0
10	N/CNT [e]	-	189.0	0	0	0

a Reaction conditions: 0.4 ml BA, 32 ml CH_3OH, 0.1 g K_2CO_3, 0.2 g catalyst, 60 ^oC, 2 MPa O_2, 12 h

b Without catalysts.

c Prepared by a CVD method using xylene as carbon source in NH_3 atmosphere at 800 ^oC. See our previous work for details.[29]

d Atomic concentration measured by XPS.

e Prepared by the same procedure but without adding $Co(OAc)_2 \cdot 4H_2O$.

The catalytic performance of CoNC/CNT and CoNC/CB were evaluated in the oxidative esterification of BA. As shown in Table 1, all cobalt containing catalysts display considerable activity. However, the control experiments without any catalyst (entry 1), with CNTs (entry 9), N-doped CNTs (entry 10) and phenanthroline modified CNTs (entry 11) are completely inactive, indicating that cobalt species are essential for the catalysis, and the nitrogen functionalities on CNTs cannot catalyze the reaction alone. Compared to XC-72R carbon black, CNTs displayed comparative performance as a support for CoNC (entry 2 and 5). This result validates the scenario using CNTs as a substitute for CB to facilitate the identification of active sites. It should be mentioned that the CoNC/CNT catalyst is highly active, even being comparable to homogeneous noble metal catalysts.[30] Considering the lack of an optimized reaction condition at present, we believe that there are still many possibilities to enhance the performance of CoNC/CNT. We also compared the performance of CoNC/CNT and FeNC/CNT. The cobalt catalyst displayed higher activity than the iron-based one, showing the promise of CoNC catalysts. (see Table S1)

It is surprising that the HCl-washing has no notable effect on the conversion of BA and MB selectivity over CoNC/CNT (entry 2 and 3), suggesting that the real active sites for the oxidative esterification are too stable to be removed by HCl. Compared with CoNC/CNT, the content of Co reduced from 1.82w% to 0.42w% after the HCl-washing, indicating that about 80% cobalt are washable and redundant for the reaction. In the case of the CB-supported catalyst, although the initial Co

content was higher, the similar fraction (~80%) of Co was washable. When a harsher washing by HNO_3 was conducted, the content of Co decreased further, because the oxidative HNO_3 may destroy the surfaces of carbon and modify surfaces of CNTs,[31] evidenced by the increase of oxygen content from 4.5% for CoNC/CNT-HCl to 5.0% for CoNC/CNT-HNO_3 measured by XPS. Significant loss of activity was observed after the HNO_3 washing (entry 4 and 7), indicating that HNO_3 could remove active cobalt species.

Table 2. Pseudo-second-order reaction rate constants and apparent activation energies of CoNC/CNT, CoNC/CNT-HCl and CoNC/CNT-HNO_3 for the oxidative esterification of BA with methanol.[a]

Catalyst	k (L mol^{-1} h^{-1}) [b]	Ea (kJ mol^{-1})
CoNC/CNT	9.2	101.5
CoNC/CNT-HCl	8.7	98.6
CoNC/CNT-HNO_3	0.49	122.0

a See Figs. S1 and S2 for detailed experimental data.

b Reaction rate constant at 60 ^{o}C.

Kinetics measurements were carried out to compare the catalytic performances of CoNC/CNT, CoNC/CNT-HCl and CoNC/CNT-HNO_3. As shown in Table 2, CoNC/CNT and CoNC/CNT-HCl show very close reaction rate constants, confirming that they qualitatively and quantitatively have the same active sites for the reaction. A drastic drop of reaction rate constant and an increase of activation energy by about 20 kJ/mol were observed upon CoNC/CNT-HNO_3, indicating the destruction of active sites under concentrated HNO_3.

Scheme 2

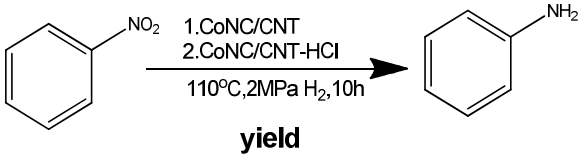

yield
1.97%
2.98%

Scheme 3

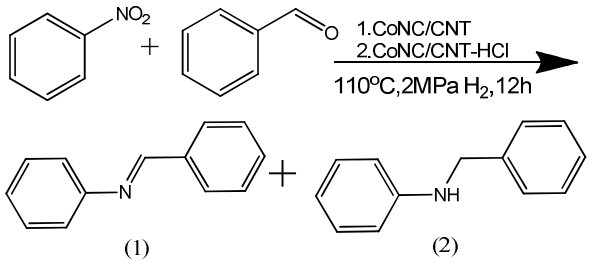

	Conv.	Selectivity (1)	Selectivity (2)
CoNC/CNT	99.8%	2.12%	97.88%
CoNC/CNT-HCl	100%	12.22%	87.78%

More reactions were conducted to compare the activities of CoNC/CNT and CoNC/CNT-HCl. Two typical hydrogenation reactions, i.e. the hydrogenation and hydrogenated coupling of nitrobenzene, were used to test the catalytic performances. Being similar to the oxidative esterification, the hydrogenation reactions display very close conversion and selectivity (see Schemes 2 and 3), indicating that the active sites survived from the HCl washing have diverse catalytic functions. Obviously, it is helpful for unravelling the active sites of these catalysts to characterize the Co species before and after acid washing.

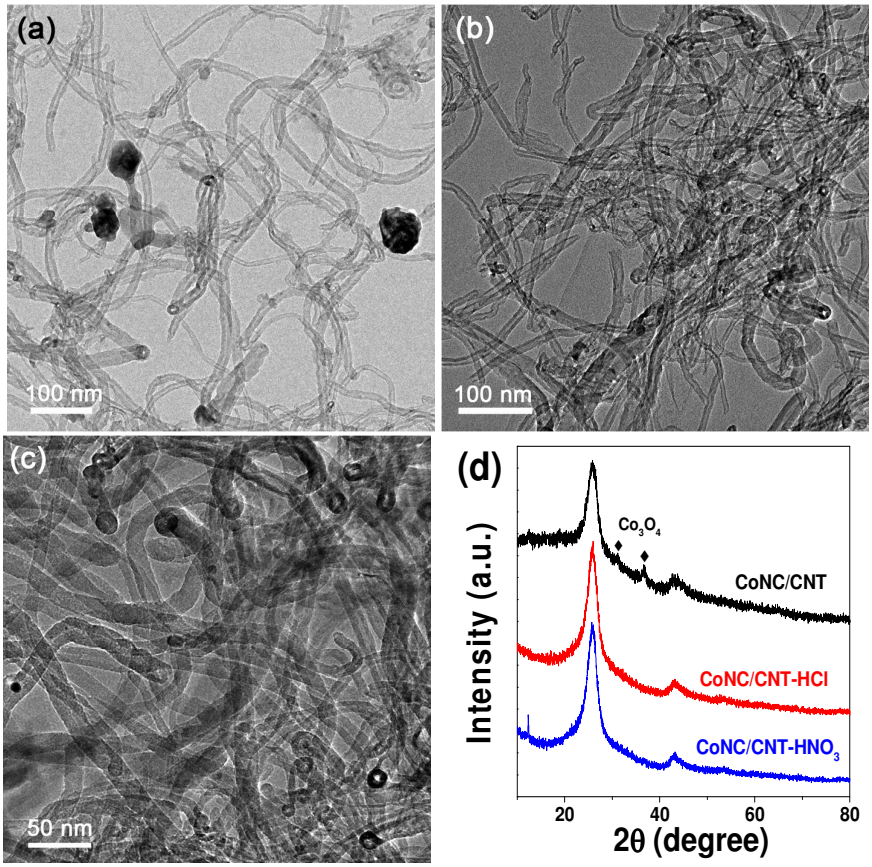

Fig.1. TEM images of (a) CoNC/CNT, (b) CoNC/CNT-HCl, (c) CoNC/CNT-HNO_3 and (d) their XRD patterns.

TEM was used to distinguish the washable inactive cobalt and the stable active one. As shown in Fig. 1a, the as-synthesized CoNC/CNT consisists of quite large paticles. However, these particulate matters completely disappeared after HCl or HNO_3 washing (Figs. 1b and 1c), suggesting that the large particles are not responsible for the catalytic activity. XRD was used to identify the composition of the large particles. As shown in Fig. 1d, the peaks from Co_3O_4 can be detected in CoNC/CNT. However, these peaks disappeared in CoNC/CNT-HCl and CoNC/CNT-HNO_3, suggesting that the washable cobalt is mainly particulate Co_3O_4.

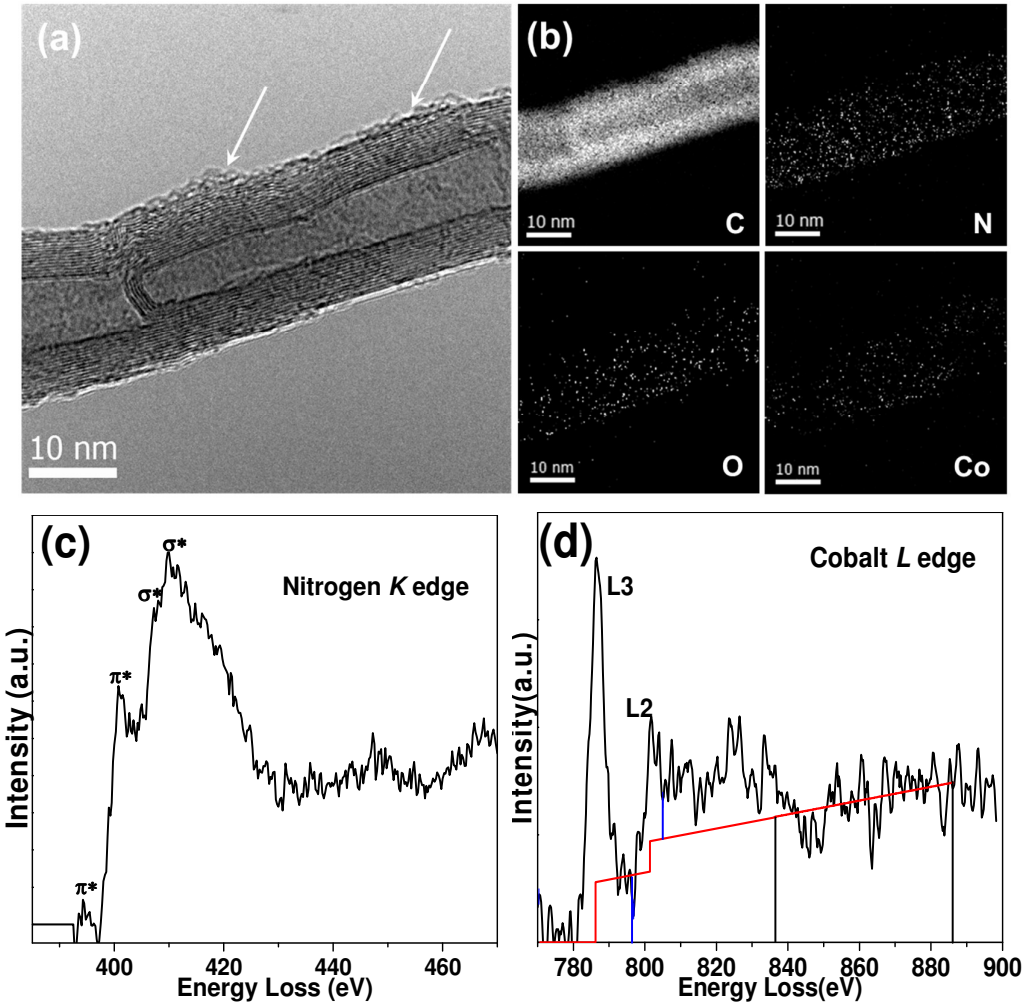

Fig.2. (a) HRTEM and (b) corresponding EFTEM images of images of CoNC/CNT-HCl. A similar result with lower magnitude is shown in Fig. S4. The white arrows indicate the defective graphenes on CNTs. (c) and (d) show the EELS spectra of nitrogen and cobalt.

Westerhaus F.A. et al.[21] have observed similar large Co_3O_4 particles on carbon-black-supported CoNC catalysts. They concluded that the Co_3O_4 particles with N-doped graphene shells are responsible for the working active sites.[23, 24] A more detailed HRTEM measurement was carried out to identify the core-shell structure. Unfortunately, this structure was so occasionally observed (see Fig. S3) that it can only be a trivial contributor to activity. It was noticed that a large amount of graphene-like debris can be found on the outer surfaces of CoNC/CNT-HCl (Figs. 2a

and S5a), which were absent in pristine CNTs, indicating that they were derived from the carbonization of 1,10-phenanthroline. Although no any Co particles can be found in this area, EDS analysis showed considerable content of Co. The distribution of C, N, O and Co was investigated by energy-filterd transmission electron microscopy (EFTEM). As shown in Fig. 2b, N, O and Co elements are homogeneously distributed on the CNT, indicating that the active cobalt is highly dispersed in the form of sub-nanometer clusters or single atom. The similar result can be obtained by STEM an EDS mapping (see Fig. S5). It is obvious that the nitrogen comes from the graphenes derived from 1,10-phenanthroline revealed by HRTEM. The strong spatial relationship between N and Co indicates that the active cobalt might be trapped on the N-doped graphenes wrapped around CNTs, not on Co_3O_4.

EELS spectroscopy was applied to reveal the valence state of N and Co. As depicted in Fig. 2c, two sharp π* peaks at about 394 and 401 eV in the N-K edge can be observed, which is due to the sp^2 bonding of N with carbon. The splitting feature of π* state is an evidence for the co-existence of two types of nitrogen, namely graphitic and pyridinic nitrogen.[32, 33] The broad peak centered around 410 eV corresponds to σ* contribution. The shoulder at 408 eV is a signature of pentagonal defect, i.e. pyrrolic nitrogen.[34] Fig. 2d shows the EELS spectrum of Co-$L_{2,3}$ edge of CoNC/CNT-HCl. The L_3/L_2 intensity ratio and distance between L_3 and L_2 lines can be used to estimate the valence state of Co.[35, 36] The L_3/L_2 ratio is determined as 3.19, and the closeness between them is 15.22 eV (see Supporting Information for details). According to the correlations established by Müller P. et al.,[36] the valence state of Co

in CoNC/CNT-HCl can be estimated between +2 and +2.66.

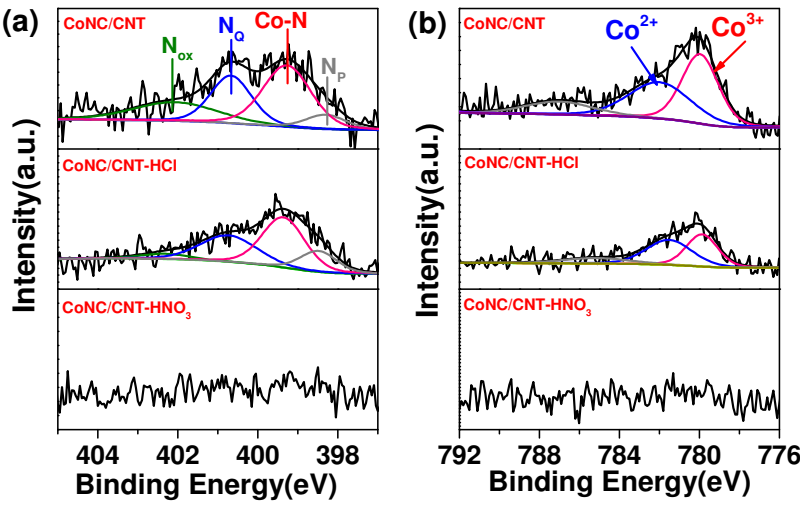

Fig.3. (a) N 1s and (b) Co 2p3/2 XPS spectra of CoNC/CNT, CoNC/CNT-HCl and CoNC/CNT-HNO_3.

Table 3 Quantitative XPS analysis for CoNC/CNT and CoNC/CNT-HCl

Catalyst	Co [a] (%)	Co^{2+} [a] (%)	Co^{3+} [a] (%)	N [a] (%)	N_P [a] (%)	CoN_x [a] (%)	N_Q [a] (%)	N_{ox} [a] (%)	TOF [b] (h^{-1})
CoNC/CNT	1.04	0.51	0.53	2.53	0.21	1.06	0.69	0.57	3315
CoNC/CNT-HCl	0.64	0.39	0.25	3.06	0.46	1.41	1.02	0.17	5207

a Atomic concentration determined by quantitative XPS analysis.

b Turnover frequency for the oxidative esterification of BA is defined as: $\frac{BA\ converted\ [mol]}{Co\ by\ XPS\ [mol]\cdot time[h]}$. The BA conversion was controlled at lower than 10 %.

Fig. 3 shows the N1s and Co2p3/2 regions of XPS spectra of CoNC/CNT, CoNC/CNT-HCl and CoNC/CNT-HNO_3. Four distinct N-functionalities can be observed in the N1s spectra of CoNC/CNT, CoNC/CNT-HCl, while no any N1s signal can be detected on CoNC/CNT-HNO_3 within the analytical depth of XPS technique, indicating that the HNO_3 treatment destroyed the N-doped graphenes. These N species can be attributed to N_P (pyridinic N, 398.3 eV), CoN_x (cobalt-coordinated N, 399.2 eV),[37] N_Q (quaternary N, 400.9 eV) and N_{ox} (N-oxides,

402.1 eV), respectively. It is interesting that CoNC/CNT-HCl has higher N content of 3.06% than that of CoNC/CNT, 2.53%. It may be caused by the re-exposure of N-functionalities on CNTs after removing Co_3O_4 particles. In both of CoNC/CNT and CoNC/CNT-HCl, the nitrogen bonded to cobalt is dominating across the four N species, indicating that the real active sites are CoN_x. Co 2p peaks of CoNC/CNT and CoNC/CNT-HCl show Co^{2+} (780.6 eV) and Co^{3+} (779.6 eV) on catalyst surfaces, accompanied by a shake-up satellite of Co^{2+} (786.3 eV).[38] The amount of Co decreased from 1.04a% to 0.64a% after HCl treatment. It was noticed that the ratio of decrements of Co^{2+} and Co^{3+} was approximately 1: 2, suggesting a stoichiometry of Co_3O_4 for the washable cobalt species. Moreover, although a mixed valence of Co was observed, a lower oxidation state of CoNC/CNT-HCl can be determined compared with CoNC/CNT, because of the higher fraction of Co^{2+}, which is consistent with EELS results.

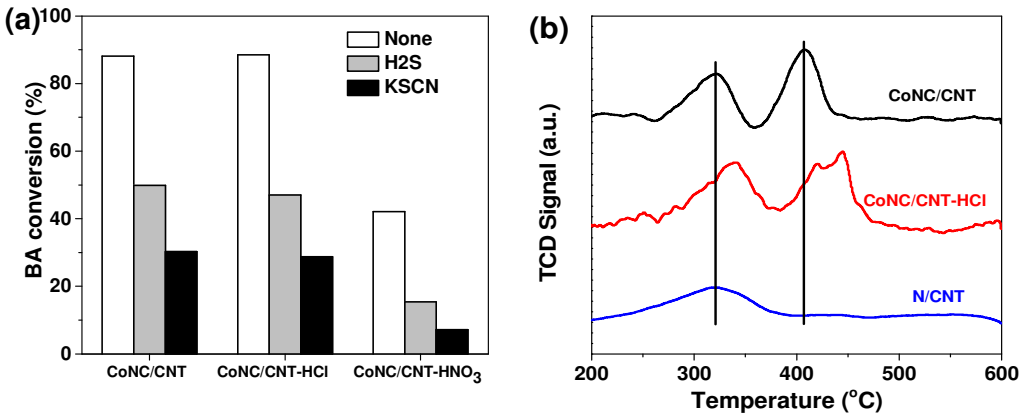

Fig.4. (a) Effect of KSCN and H_2S as poisons on the BA conversion in its oxidative esterification with methanol over CNT-supported catalysts. Reaction conditions: 0.4 ml benzyl alcohol, 32 ml CH_3OH, 0.1 g K_2CO_3, 60 ^oC, 2 MPa O_2, 12 h. (b) H_2S-TPD profiles of CoNC/CNT, CoNC/CNT-HCl and N/CNT.

Poisoning experiments were carried out to further prove the involvement of the highly dispersed Co in the catalysis. CN^-, SCN^- or H_2S have been demonstrated to be capable of bonding with transition metal-centered active sites and deactivate them.[39-41] In this work, we examined the active cobalt sites by poisoning them with KSCN and H_2S. As shown in Fig. 4a, KSCN in reactants and the pre-adsorbed H_2S significantly deactivate the CNT-supported catalysts, suggesting the interaction between the sulfur-containing poisons and active sites containing cobalt. Moreover, a HRTEM measurement and EFTEM analysis for the catalyst poisoned by KSCN revealed a homogeneous profile of sulfur over CNTs. (see Fig. S6) The high spatial relevance with Co is indicative of the adsorption of SCN^- over Co sites.

H_2S-TPD was carried out to investigate the interaction between the active sites and H_2S as poison. As shown in Fig. 4b, two distinct desorption peaks, centered at 320 ^oC and 405 ^oC, can be observed for CoNC/CNT. After washed by HCl, the two peaks remain, but shift toward higher temperatures by about 20 ^oC, indicating the stronger adsorption. The similar H_2S-TPD behavior has been reported by Singh D et al. for FeNC catalysts for ORR reaction.[40] The peak at 320 ^oC origins from H_2S adsorbed over N-functionalities of N-CNTs. It can be supported by the TPD profile of N/CNTs, which shows the similar desorption peak. However, no any peaks can be detected for pristine CNTs. (see Fig. S7) This result also suggests that the peak at higher temperature is due to the stronger adsorption of H_2S over Co sites, which may interfere the coordination between transition metal and pyridinic nitrogen and deactivate the catalyst, being similar to the deactivation behavior of FeNC for ORR.

[40] It is noticeable that the intensity of high-temperature peak remains same after HCl washing, indicating the high stability of active sites as revealed by the catalytic results.

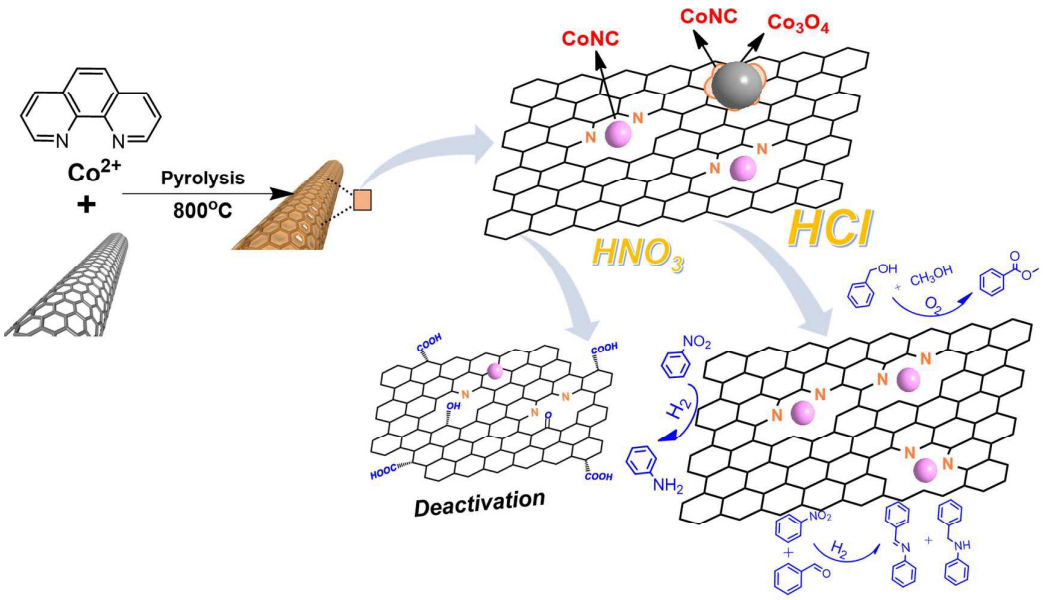

Fig.5 Schematic diagram for the formation of CoNC active sites for the BA oxidative esterification, NB hydrogenation and hydrogenated coupling with BDH.

Above results clearly indicate that, although there are two types of Co species on CNTs, i.e. the large Co_3O_4 particles and sub-nanometer CoNC, the active sites are composed of cobalt bonded to nitrogen of N-doped graphene derived from 1,10-phenanthroline. G. Zhu et al.[42] also raised the similar active sites which are CoNx (maybe Co-N_4) supported on porous materials synthesized by carbonization of Co-MOF. A schematic mechanism was proposed to elucidate the formation of the active sites. As shown in Fig. 5, 1,10-phenanthroline is carbonized to form N-doped graphene sheets wrapped on CNTs at 800 °C. Because of the strong chelation between Co^{2+} and 1,10-phenanthroline, cobalt can be stabilized by the nitrogen sites, probably pyridinic nitrogen, during the pyrolysis, which results in the generation of

the homogeneously distributed Co sites on atomic/subnanometer scale. These sites are characterized by the high dispersion, bonding to N atoms and thereby the excellent catalytic activity analogous to well-defined molecular catalysts. On the other hand, the decomposition of excess $Co(OAc)_2$ leads to the formation of particulate Co_3O_4, around which the graphene sheets derived from 1,10-phenanthroline can be formed either. It cannot be excluded that CoNx embedded in graphene shells encapsulating Co_3O_4 particles might contribute to the activity to some extent, however, its effect should be marginal because of the relatively low surface area of Co_3O_4 particles. The Co_3O_4 particles and graphenes on their surfaces cannot survive from the HCl washing, after which the catalysts with homogeneous Co active sites can be obtained. This catalyst is active in diverse organic synthetic reactions. Washing with HNO_3 is detrimental to the activity, because HNO_3 can oxidatively remove the graphenes containing active Co. This can be supported by the reduction of Co content and the decreased defectiveness of carbon revealed by Raman spectroscopy. (see Fig. S7)

It is highly desired to understand the molecular structure of active sites. A deduction was made through the quantitative XPS results. Assuming that all Co atoms on CoNC/CNT-HCl are active, the N/Co ratio of active sites can be estimated as 2.2 (Table 3), where only the nitrogen bonded to Co is considered. Although the precise molecular structure of the active sites is unclear yet, this value implies that cobalt chelate complex with 2 to 3 nitrogens in graphene lattice, probably like the pyridinic vacancy, might be responsible for the activity. By combining the

quantitative XPS data with specific surface area, the intrinsic catalytic activity for the oxidative esterification of BA can be estimated. High TOF values up to 3300 and 5200 h^{-1} were measured for CoNC/CNT and CoNC/CNT-HCl, respectively, as shown in Table 3. More experiments are needed to resolve the structure in the future.

4. Conclusions

In conclusion, a simple acid-washing method was used to distinguish the heterogeneity of cobalt species of CoNC/CNT catalyst. It was found that Co_3O_4 particles that can be removed by HCl washing have no effect on the activity. The real active cobalt species are highly dispersed on CNTs on atomic or subnanometer scale, which are stable under HCl condition. The structure of active sites is proposed as a cobalt chelate complex embedded in pyridine-like vacancies of N-doped graphenes created by the thermolysis of cobalt salts and 1,10-phenanthroline. The new insight into the active sites of carbon supported CoNx catalysts may lead to a rational design of high-performance catalysts in the future.

Acknowledgements

This work was supported by the National Natural Science Foundation of China (Nos. 21133010, 21273079), the Guangdong Provincial Natural Science Foundation (Nos. S20120011275, 2014A030312007), Program for New Century Excellent Talents in University (NCET-12-0190) and the Fundamental Research Funds for the Central Universities of China (Nos. 2014ZG0005, 2015PT012).

References

1. Y. Zhu and Y. Wei, *RSC Adv.*, 2013, **3**, 13668-13670.

2. X.-F. Wu and C. Darcel, *Eur. J. Org. Chem.*, 2009, 1144-1147.

3. Y. Li, S. Yu, X. Wu, J. Xiao, W. Shen, Z. Dong and J. Gao, *J. Am. Chem. Soc.*, 2014, **136**, 4031-4039.

4. K. Junge, K. Schroder and M. Beller, *Chem. Commun*, 2011, **47**, 4849-4859.

5. F. G. Gelalcha, B. Bitterlich, G. Anilkumar, M. K. Tse and M. Beller, *Angew. Chem. Int. Ed.*, 2007, **46**, 7293-7296.

6. G. Anilkumar, B. Bitterlich, F. G. Gelalcha, M. K. Tse and M. Beller, *Chem.Commun* 2007, 289-291.

7. K. Schröder, S. Enthaler, B. Join, K. Junge and M. Beller, *Adv. Synth. Catal.*, 2010, **352**, 1771-1778.

8. S. Kanemasa, Y. Oderaotoshi, S. Sakaguchi, H. Yamamoto, J. Tanaka, E. Wada and D. P. Curran, *J. Am. Chem. Soc.*, 1998, **120**, 3074-3088.

9. J. L. Carsten Bolm, Jacques Le Paih, and Lorenzo Zani, *Chem. Rev.*, 2004, **104**, 6217-6254

10. A. Vaccari, *Catal. Today*, 1998, **41**, 53-71.

11. A. Vaccari, *Appl. Clay. Sci.*, 1999, **14**, 161-198.

12. F. Bedioui, *Coord. Chem. Rev.*, 1995, **144**, 39-68.

13. R. F. Parton, I. F. J. Vankelecom, D. Tas, K. B. M. Janssen, P.-P. Knops-Gerrits and P. A. Jacobs, *J. Mol. Catal. A: Chem.*, 1996, **113**, 283-292.

14. R. Augustine, S. Tanielyan, S. Anderson and H. Yang, *Chem. Commun*, 1999, 1257-1258.

15. C. Freire, C. Pereira and S. Rebelo, *Catalysis*, 2012, **24**, 116-203.

16. A. Morozan, P. Jegou, B. Jousselme and S. Palacin, *Phys. Chem. Chem. Phys.*, 2011, **13**, 21600-21607.

17. S. Deng, P. Yuan, X. Ji, D. Shan and X. Zhang, *ACS Appl. Mater. Inter.*, 2015, **7**, 543-552.

18. W. Feng and P. Ji, *Biotechnol. Adv.*, 2011, **29**, 889-895.

19. R. V. Jagadeesh, H. Junge, M. M. Pohl, J. Radnik, A. Bruckner and M. Beller, *J. Am. Chem. Soc.*, 2013, **135**, 10776-10782.

20. R. V. Jagadeesh, A. E. Surkus, H. Junge, M. M. Pohl, J. Radnik, J. Rabeah, H. Huan, V. Schunemann, A. Bruckner and M. Beller, *Science*, 2013, **342**, 1073-1076.

21. F. A. Westerhaus, R. V. Jagadeesh, G. Wienhöfer, M.-M. Pohl, J. Radnik, A.-E. Surkus, J. Rabeah, K. Junge, H. Junge, M. Nielsen, A. Brückner and M. Beller, *Nat.Chem.*, 2013, **5**, 537-543.

22. D. Banerjee, R. V. Jagadeesh, K. Junge, M. M. Pohl, J. Radnik, A. Bruckner and M. Beller, *Angew. Chem. Int. Ed.*, 2014, **53**, 4359-4363.

23. T. Stemmler, F. A. Westerhaus, A.-E. Surkus, M.-M. Pohl, K. Junge and M. Beller, *Green Chem.*, 2014, **16**, 4535-4540.

24. R. V. Jagadeesh, H. Junge and M. Beller, *ChemSusChem*, 2015, **8**, 92-96.

25. R. V. Jagadeesh, T. Stemmler, A.-E. Surkus, H. Junge, K. Junge and M. Beller, *Nat. Protoco*, 2015, **10**, 548-557.

26. S. Pisiewicz, T. Stemmler, A.-E. Surkus, K. Junge and M. Beller, *ChemCatChem*, 2015, **7**, 62-64.

27. J. Deng, H.-J. Song, M.-S. Cui, Y.-P. Du and Y. Fu, *ChemSusChem*, 2014, **7**, 3334-3340.

28. Y. Wu, Q. Shi, Y. Li, Z. Lai, H. Yu, H. Wang and F. Peng, *J. Mater. Chem. A*, 2015, **3**, 1142-1151.

29. Y. Cao, H. Yu, J. Tan, F. Peng, H. Wang, J. Li, W. Zheng and N.-B. Wong, *Carbon*, 2013, **57**, 433-442.

30. C. Liu, J. Wang, L. Meng, Y. Deng, Y. Li and A. Lei, *Angew. Chem. Int. Ed.*, 2011, **50**, 5144-5148.

31. L. Jie, A. G. Rinzler, D. Hongjie, J. H. Hafner, R. K. Bradley, P. J. Boul, A. Lu, T. Iverson, K. Shelimov, C. B. Huffman, F. Rodriguez-Macias, S. Young-Seok, T. R. Lee, D. T. Colbert and R. E. Smalley, *Science*, 1998, **280**, 1253-1256.

32. M. Terrones, P. M. Ajayan, F. Banhart, X. Blase, D. L. Carroll, J. C. Charlier, R. Czerw, B. Foley, N. Grobert, R. Kamalakaran, P. Kohler-Redlich, M. Rühle, T. Seeger and H. Terrones, *Appl. Phys. A*, 2002, **74**, 355-361.

33. H. Lin, R. Arenal, S. Enouz-Vedrenne, O. Stephan and A. Loiseau, *J. Phys. Chem. C*, 2009, **113**, 9509-9511.

34. R. Arenal, K. March, C. P. Ewels, X. Rocquefelte, M. Kociak, A. Loiseau and O. Stéphan, *Nano Lett.*, 2014, **14**, 5509-5516.

35. Z. L. Wang, J. S. Yin and Y. D. Jiang, *Micron.*, 2000, **31**, 571-580.

36. P. Muller, M. Meffert, H. Stormer and D. Gerthsen, *Microsc. Microanal.*, 2013, **19**, 1595-1605.

37. J. M. Ziegelbauer, T. S. Olson, S. Pylypenko, F. Alamgir, C. Jaye, P. Atanassov

and S. Mukerjee, *J. Phys. Chem. C*, 2008, **112**, 8839-8849.

38. T. J. Chuang, C. R. Brundle and D. W. Rice, *Surf. Sci.*, 1976, **59**, 413-429.

39. M. S. Thorum, J. M. Hankett and A. A. Gewirth, *J. Phys. Chem. Lett.*, 2011, **2**, 295-298.

40. D. Singh, K. Mamtani, C. R. Bruening, J. T. Miller and U. S. Ozkan, *ACS Catal.*, 2014, **4**, 3454-3462.

41. S. Gupta, C. Fierro and E. Yeager, *J.Electroanal.Chem.Interfac.*, 1991, **306**, 239-250.

42. G. Yu, J. Sun, F. Muhammad, P. Wang and G. Zhu, *RSC Advances*, 2014, **4**, 38804-38811.

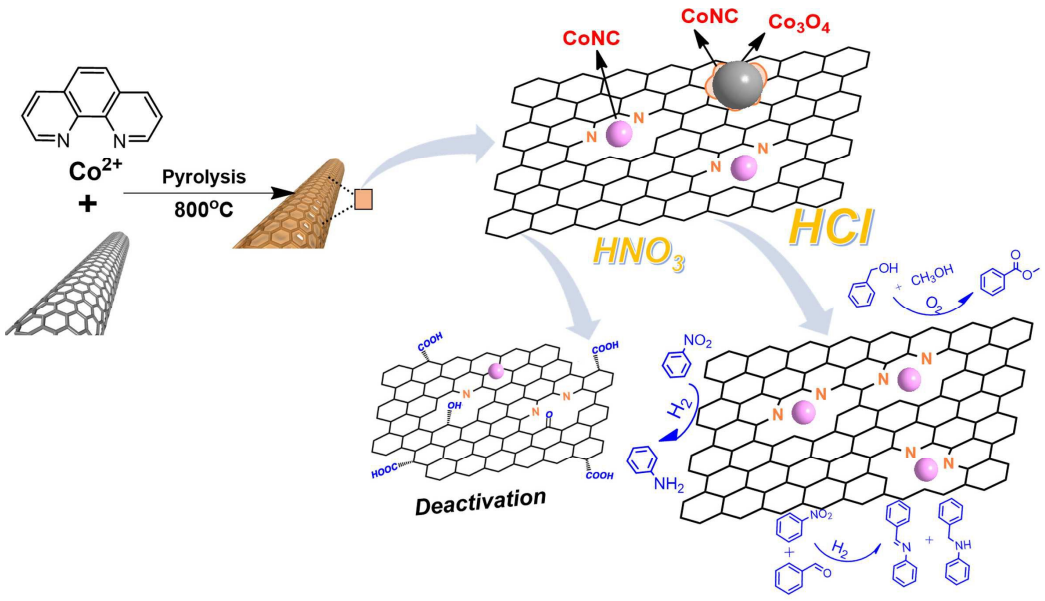

Cobalt chelate complexes bonded to 2 to 3 nitrogens in graphene lattice are the active sites for the oxidative esterification of benzyl alcohol by molecular oxygen, the selective reduction of nitrobenzene by hydrogen and the hydrogenated coupling of nitrobenzene and benzaldehyde.